POLITECNICO DI TORINO
Repository ISTITUZIONALE

Thermochromic photoluminescent 3D printed polymeric devices based on copper-iodide clusters

Terms of use:

(Article begins on next page)

20 March 2024

Research paper

Thermochromic photoluminescent 3D printed polymeric devices based on copper-iodide clusters

Matteo Gastaldi [a], Ignazio Roppolo [b, c], Annalisa Chiappone [b, c], Claudio Garino [a], Andrea Fin [d], Matteo Manachino [e], Paolo Sirianni [f], Guido Viscardi [a], Luciano Scaltrito [b], Marco Zanetti [a, g], Silvia Bordiga [a], Claudia Barolo [a, g]

[a] Department of Chemistry and NIS Interdepartmental Centre and INSTM Reference Centre, University of Torino, Via Pietro Giuria 7, 10125 Torino, Italy

[b] Department of Applied Science and Technology, Politecnico di Torino, Corso Duca degli Abruzzi 24, 10129 Torino, Italy

[c] Center for Sustainable Future Technologies, Istituto Italiano di Tecnologia, Via Livorno 60, 10144 Torino, Italy

[d] Department of Drug Science and Technology, University of Torino, Via Pietro Giuria 11, 10125 Torino, Italy

[e] Chilab-Materials and Microsystems Laboratory, Department of Applied Science and Technology (DISAT), Politecnico di Torino, Via Lungo Piazza d'Armi 6, 10034 Torino, Chivasso, Italy

[f] Microla Optoelectronics S.r.l., Via Le Chiuse 101, 10144 Torino, Italy

[g] ICxT Interdepartmental Center, University of Turin, Lungo Dora Siena 100, 10153 Torino, Italy

ARTICLE INFO

ABSTRACT

In this work, optically active devices are fabricated by Digital Light Processing (DLP) 3D printing technology employing copper-iodide photoluminescent clusters as smart dyes in the photocurable formulation. These compounds are easy to synthesize, low cost and possess large stoke shift, thermochromic and rigidochromic properties, which make them particularly appealing for the development of optical devices. By dispersing such compounds in photocurable formulations, the same properties are transferred to polymeric materials, enabling the production of a large range of devices. Absorbing in the UV range and emitting in the visible range, those clusters show twofold advantages: on the one hand, competing with the photoinitiator for the light absorption, they allow a better control of the photopolymerization process, enabling the fabrication of precise structures; on the other hand, these possess aesthetic properties, being transparent and then emitting light when irradiated. At last, functional structures, such as 3D printed polymeric waveguides (PWGs) and downshifting devices, are fabricated and investigated but even other uses can be envisaged, such as cryogenic optical thermometers.

1. Introduction

Polymeric photoluminescent waveguides (PWGs) are nowadays used in a broad range of applications, such as in light-emitting devices (LEDs) [1], light-tunable photonics [2,3], optics [4], photonic integrated circuits [5], communications [6], biomedicals [7,8] and even sensors [9–12]. The possibility to exploit the thermal and mechanical stability of the polymeric matrices, joined to the flexibility of the final device and the inexpensiveness of the materials, has promoted the use of polymers as materials for innovative waveguides [10] but still a lot can be done, especially in the fabrication complex devices.

In the last 30 years, many fabrication processes have been developed to shape those materials, such as lithography [5], controlled deposition [13] and electrospinning [14]. Generally, PWGs are fabricated employing conjugated polymers, that emit thanks to the long-range π-electron conjugation [15]. This strategy is largely explored, however it

presents some drawbacks, such as high costs, the necessity of usually complex chemical synthesis, the not-trivial relationships between structure and properties [16,17], the limits of the manufacturing methods [18] and finally the presence of amorphous domains and defects [19]. An alternative method to produce PWGs consists in the dispersion of photoluminescent fillers, such as organic or inorganic molecules and complexes, in an optically inert polymeric matrix. The use of this loading method may lead to several advantages like high optical transparency, reduced costs and easy processability [15].

With the recent improvement of 3D printing technologies, it has become easier to build really customized optical elements with complex three-dimensional shapes, maintaining high fidelity to the CAD virtual project. Additional functionalities can be also conferred through the synthesis and development of functional and printable polymeric materials [20] with the introduction of dyes and fillers, as reported in some recent reviews [21–23].

Typically, three-dimensional printed (3DP) PWGs were produced using Fused Filament Fabrication (FFF) [24–26] or Direct Ink Writing (DIW) [27] techniques. In those cases, the emitting properties were obtained introducing transition metals [28], rare earth [29,30] and organo-lanthanide complexes [31] or organic molecules [32] as guests. Only recently, the use of such compounds has found applications in light induced 3D printing (which comprehends Stereolithography (SLA) and in Digital Light Processing (DLP) printers) to obtain colored emitting polymers [20] with complex and accurate shapes [33]. As an example, Frascella et al. [34] demonstrated the possibility to fabricate PWGs using DLP, copolymerizing an organic emitter with an optically inert polymer. However, the residual-colored matrix and the reduced Stokes shift of the photoluminescent moieties represent a limit in the use of this 3DP material as PWGs.

The application of a printable polymeric matrix embedding emitters that are able to absorb in the UV range and emit in the visible range, showing high stability under light irradiation, high quantum yield and very low costs can represent a step forward in the realization of efficient PWGs. Thanks to DLP method and the possibility to easily customize the material's properties playing on the different components [35], very complex and high-defined devices can be carried out [20].

Furthermore, light sensitive compounds can play a twofold positive effect in materials for light-induced 3D printing: on the one hand, those can impart new functionalities, even at relatively low amounts, on the other, those can be used to improve the printing precision, controlling the light absorption and thus the photopolymerization process, avoiding uncontrolled curing [23]. Example of this twofold use can be found in many applications, such as laser-tunable elastic modulus [35], photo-activated gas permeability [36], light-emitting materials [20] and UV or temperature-responsive polymers [37]. Moreover, since light-based 3D printers operates at room temperature, any temperature-induced dye degradation can be avoided. Unfortunately, dyes may reduce the transparency of the structures, conferring a color to the polymeric matrix, which can be highly undesired, especially in optical applications.

In this work, we investigated the introduction of copper iodide clusters, of general formula [$Cu_4I_4L_4$] (L = phosphine-based ligands, Fig. 1), in an acrylic 3DP polymeric matrix able to guide the irradiation from one end to the other, converting it from UV to visible light. Copper-halide based clusters are well-known and deeply studied compounds to produce luminescent materials [38], thanks to their intriguing thermal-depending photophysical properties [39–42] according to the different ligands used [43]. These species are stimuli responsive since they can change their emission according to environmental, mechanical and temperature variations [44,45]. Furthermore, these compounds display very high quantum yields [46], an absorption band in the UV range, a large Stokes shift, high stability, in particular for compounds containing iodine, and they also show mechanochromic and rigidochromic behaviors [47]. Moreover, the low toxicity of these compounds, compared to other transition metals, the facile synthesis with good yield and the peculiar optical properties of these compounds make them very promising in the use as thermometer [46] or in many other applications [43,48]. In this context, these compounds are suitable to generate almost transparent PWGs.

3D printable resins were carried out to investigate the photopolymerization kinetics and optical properties of the bisphenol A ethoxylate diacrylate (BEDA), used as printable monomer, containing different concentrations of copper-iodide clusters as smart dyes. Then, the 3D printing process was performed, finding the optimal parameters to fabricate precise complex devices that were fully characterized, taking in particular account optical and emissive properties. The high resolution achieved for the final device and the ability to guide the irradiation through the polymeric medium with a good efficiency was also demonstrated, as well as the relative effect of temperature on the guiding efficiency. To the best of our knowledge, this is the first time that copper-based clusters are introduced in 3D printable formulations.

2. Experimental section/methods

2.1. Materials

Bisphenol A ethoxylate diacrylate (BEDA) (Mn = 512, EO/phenol = 2), 2-hydroxy-2-methylpropiophenone (HMPP), toluene, chloroform, dichloromethane (DCM) and acetonitrile (ACN) were purchased from Sigma-Aldrich and used as received. The two copper iodide clusters [$Cu_4I_4(PPh_3)_4$] 1 and [$Cu_4I_4(PPh_2(CH_2)_2CH_3)_4$] 2 depicted in Fig. 1 were synthetized according to the procedures and matched the reported characterizations [44,49].

3. Formulations

Six formulations containing different concentration (0.1%, 1.0% and 5.0% w w^{-1}) of each copper-based cluster were prepared as follows. Each cluster was introduced as solid in a vial (10 mL) containing BEDA (5.0 g) liquid monomer. DCM (1.0 mL) was introduced into the formulation and all the vials were stirred for 1 h at 50 °C and then sonicated in an ultrasonic bath for 1 h more, until homogeneous solutions were obtained. The same procedure was followed to prepare a blank formulation without the introduction of copper cluster, used as refer-
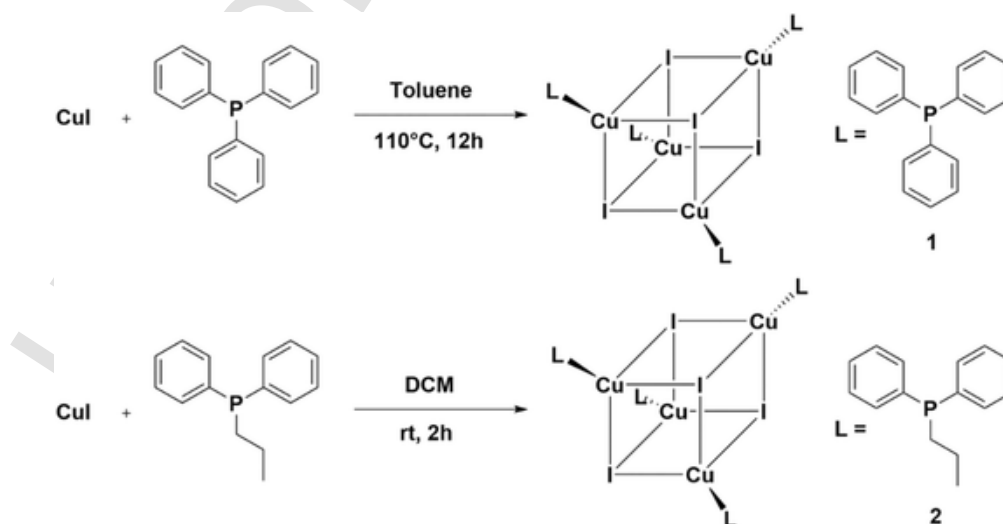

Fig. 1. Synthesis of copper-based clusters.

ence. Before printing, the photoinitiator was added (1.0% w w^{-1}) and the solution was sonicated for 5 min more.

4. 3D printing process

The printing process was carried out with Asiga DLP-3D printer (Max-UV) with nominal X–Y pixel resolution of 27 μm and the minimum Z-axis control of 1 μm. Light intensity of 25 mW cm^{-2} and layers slicing of 25 μm were the optimal parameters for the 3D printing process. The first 3 layers were irradiated for 15 s, to ensure the adhesion on the building platform. The irradiation exposure time was reduced to 10 s for all other layers. The printing process was performed a 25 °C and a post-curing process (5 min each side) was carried out in a UV oven by Robofactory (light intensity 10 mW cm^{-2}) to obtain the almost total conversion of acrylic double bonds.

5. Characterization

^{1}H, ^{13}C and ^{31}P NMR spectra were recorded on a JEOL ECZR600 FT NMR spectrometer (^{1}H operating frequency 600 MHz) at 313 K and 298 K for 1 and 2, respectively. ^{1}H and ^{13}C chemical shifts are reported relative to TMS ($\delta = 0$) and referenced against solvent residual peaks. Toluene-d_8 deuterated was used as deuterated solvent for 1, while for 2 chloroform-d was employed.

UV-Visible absorption spectra were recorded on polymeric films in the 250–750 nm range with a Varian Cary 300 spectrophotometer. Photoemission spectra, luminescence lifetimes and quantum yields were acquired with a HORIBA Jobin Yvon IBH Fluorolog-TCSPC spectrofluorometer, equipped with a Quanta-φ integrating sphere. Solid state measurements were performed on 3D printed polymeric strips.

Photorheological tests were performed in real time during irradiation using an Anton Paar rheometer (Physica MCR 302) equipped with a Hamamatsu LC8 lamp (light emission in the UVA range, intensity 25 mW cm^{-2}). The measurements were performed in a plate-plate geometry equipped with quartz bottom plate. The gap between the plates was 200 μm. Oscillatory measurements were performed at 25 °C, at constant frequency (1 Hz) and amplitude (1%). Amplitude sweep test (from 0.01% to 100%, frequency 1 Hz) was preliminarily performed to evaluate the linear viscoelastic range.

ATR-FTIR spectra were collected with a Nicolet iS50 Spectrometer equipped with an attenuated total reflection (ATR). The range 4000–500 cm^{-1} was scanned (32 scans per spectra, resolution 2 cm^{-1}).

The acrylic double bond conversion after the different stages was determined by the reduction of the peak centered at 980 cm^{-1} normalized by the aromatic signal at 1550 cm^{-1}.

Differential scanning calorimetry (DSC) measurements were performed with a Q200 (TA Instrument). The experiments were carried out between - 20–80 °C with a heating rate of 20 °C min^{-1} and 10 °C min^{-1} as cooling rate. Thermal gravimetric analyses (TGA) were carried out

with a Q600 (TA Instrument) on the polymeric film heating from 30 °C to 650 °C with a heating rate of 10 °C min^{-1} in air.

Insoluble fraction was measured by evaluating the weight loss of 3DP components after 24 h of chloroform extraction.

The precision of 3D printing process was evaluated using a E4 3D scanner (3Shape) with scanning accuracy of 4 μm.

The efficiency of the light propagation into the PWGs were evaluated using, as optical power source, a high flux density 365 nm surface mount ceramic package UV LED with integrated flat glass lens (LZ4–04UV0R OSRAM). The current source and voltage meter is a KEITHLEY 2602 A SourceMeter. The spectrometer is an AcalBFi USB4000 preconfigured for applications from 200 to 850 nm and the multimode optical fiber is a FT600EMT with numerical aperture of 0.39 and diameter of 600 μm.

6. 3. Result and discussion

Two different copper-based clusters were synthetized to evaluate their dispersion into liquid formulations composed of BEDA as monomer and HMPP as photoinitiator. Both of the synthetized compounds have been considered in previously reported papers [39,43–45, 47,49,50] and their synthetic schemes are reported in Fig. 1. Despite the higher temperature and times needed to produce 1, it presents higher quantum yield than 2 and it can be excited with a more UV-shifted wavelength [49].

Different formulations were set up to evaluate the optimal concentration of copper clusters into the polymeric BEDA matrix. Low amounts of DCM were added in preparation step to dissolve the clusters' aggregates. Furthermore, due to its high volatility, this solvent evaporates during mixing and 3D printing processes, not affecting printable formulations. Nevertheless, copper cluster 1 presented some solubility issues, due to its low solubility in almost every organic solvent at room temperature. A good dispersion was achieved only for 0.1% w w^{-1}, while for the formulation containing higher concentration, a large amount of cluster remained undissolved, making the resins cloudy (Fig. 2a). UV irradiation at 365 nm emphasizes these solubility problems as depicted in Fig. 2b in which a yellow emission can be detected only for 1.0% w w^{-1} and 5.0% w w^{-1} of 1. In the case of compound 2, all the solutions do not show any emitting property, demonstrating the excellent solubility into the liquid resin. In fact, as previously reported, both 1 and 2 are able to emit only in crystalline solid state, while they almost lose this property in solution [49], as demonstrated by the emission spectra of liquid formulation containing 1.0% w w^{-1} of both 1 and 2 (Fig. S1). In this graph the insolubility of 1 is clearly visible by the emission spectrum while 2 is totally soluble and no emitting properties can be detected.

Based on these initial results, some photopolymerization tests were carried out irradiating the resulting formulations, except for 5.0% w w^{-1} of 1, with UV light under inert atmosphere, to evaluate the homo-
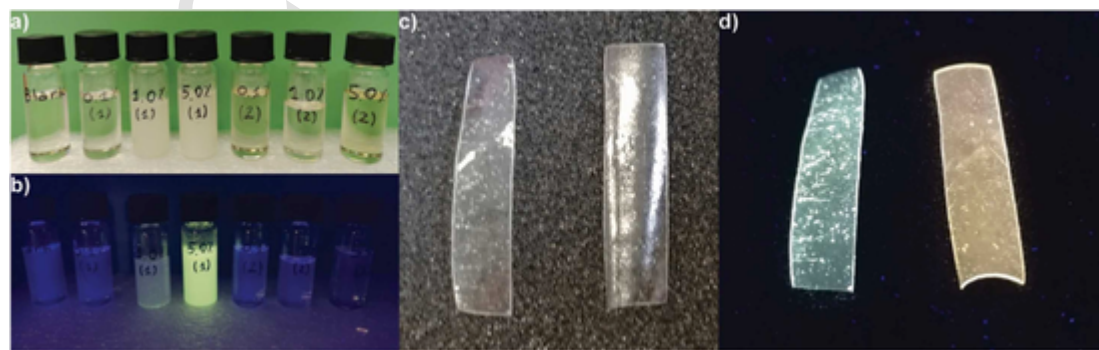
Fig. 2. Formulations of monomer, photoinitiator, DCM and different concentrations of 1 and 2 under (a) ambient illumination and (b) under 365 nm UV lamp. The presence of insolubilized copper cluster is detected by the yellow emission of compound powder. c) Polymeric films with 1.0% w w^{-1} of both copper clusters 1 (left) and 2 (right). d) Emission of polymeric films with 1.0% w w^{-1} of 1 (left) and 2 (right) under 365 nm light.

geneity of the resulting films. All films (Fig. S2) appeared transparent under ambient illumination and only the formulations containing up to 1.0% w w^{-1} of 1 produced a precipitation of the copper cluster into the polymeric solid matrix, as demonstrated by Fig. 2c-d compared to the film with the same concentration of 2 under 365 nm lamp.

As depicted in Figs. S3, 1 presents higher emission at 330 nm excitation wavelength, but unfortunately very low solubility, which in turns induces low stability in the formulations during the printing. For these reasons, the following 3D printing process and all experiments were conducted only applying compound 2.

Our previous results using conventional UV curing demonstrated that the introduction of less than 5.0% w w^{-1} of copper clusters do not affect consistently the acrylic double bond conversion and the transparency [38]. Based on this report, different formulations were investigated by photorheology tests to evaluate the polymerization kinetics and transparency of the resulting 3DP films. As depicted in Fig. 3a, the introduction of 1.0% w w^{-1} of 2 leads to almost transparent polymeric films that start to absorb irradiation under 400 nm. In the same figure, the absorption spectrum of the HMPP photoinitiator is reported, showing an absorption profile that overlaps the copper-iodide cluster one. This overlapping can be useful in our process to control the printing precision and to avoid layers undesired curing out of the exposed areas [23]. The transparency is preserved after the post-curing process (Fig. S4).

The effect of the concentration of 2 on the photopolymerization kinetics can be evaluated by photorheology tests. As depicted in Fig. 3b, the presence of the copper cluster 2 does not affect the photopolymerization up to a concentration of 5.0% w w^{-1} at the LED power

(25 mW cm^{-2}) of the printer. This liquid mixture showed a higher storage modulus (G′), meaning a higher viscosity conferred by the cluster and a delayed start of the photopolymerization reaction with respect to other formulations.

Moreover, a lower value of G′ is reached after irradiation, that may be consistent with a reduced photopolymerization efficiency and a lower conversion of acrylic double bonds. These phenomena can be ascribed to the concurrent absorption of UV light between the photoinitiator and the emitter, which decreases the rate of photoinitiation and thus the final conversion.

To evaluate the real effect of 2 on the photopolymerization kinetics, photorheology tests were repeated at lower light intensity (0.5 mW cm^{-2}). In these conditions, the delayed start of photopolymerization for each formulation (Fig. S5) was observed, indicating a clear effect of the copper clusters. On the other hand, all the considered formulations of copper cluster, including the one with 5.0% w w^{-1}, show good transparency in the visible range, and this property is preserved in the 3DP matrices (Fig. 3c).

3DP PWGs with an increasing content of 2 were produced, evaluating the good final resolution and their visible emitting properties under UV irradiation (Fig. 3d). The blank and the sample containing 0.1% w w^{-1} of 2 show a blue emission due to the polymeric matrix (Fig. S6) while with the addition of 1.0% of 2 the emission start tuning to light yellow, reaching the maximum at 5.0% w w^{-1}. With 1.0% w w^{-1} good emitting properties can be reached avoiding the efficiency reduction on the photopolymerization kinetics and preserving at the same time the mechanical and thermal properties of the polymeric matrix. The fabrication of these samples and the evaluation of the double bond conver-
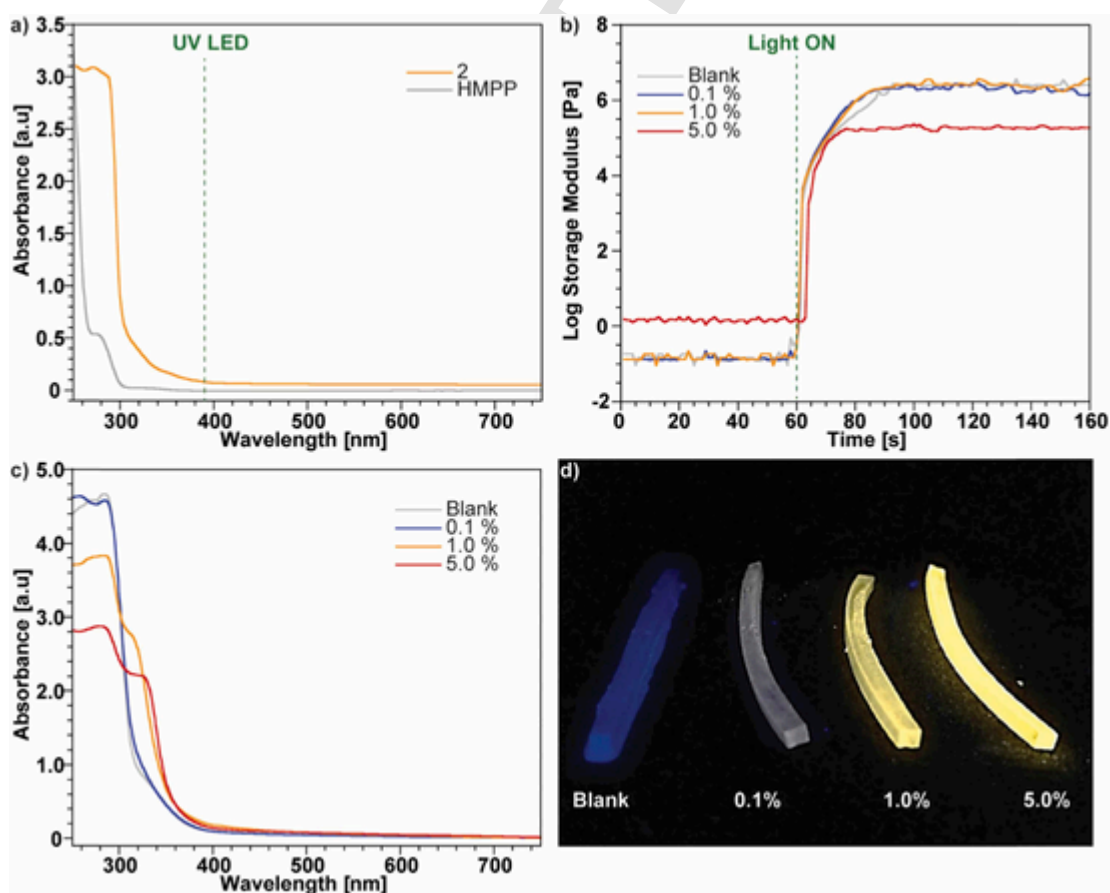

Fig. 3. a) UV-Visible spectra of 3DP polymeric film containing 1.0% w w^{-1} of 2 overlapped to UV spectrum of photoinitiator in ACN. The UV emission of DLP 3D printer (385 nm) is represented by the straight dashed green line. b) Photorheological curves of liquid formulations containing increasing concentrations of 2. The formulation without copper cluster represented the reference (Blank). c) UV-Visible spectra of 3D printed films containing different concentrations of 2. d) Picture of 3DP polymeric strips with an increasing concentration of 2 under UV (365 nm) light.

sion allow the optimization of the 3D printing parameters, reported in Table 1.

To evaluate the efficiency of 3DP process, the acrylic double bonds conversion was evaluated by means of ATR-FTIR spectroscopy (the overlapped spectra are reported in Fig. S7). As reported in Table 1, the presence of copper clusters did not affect the conversion after 3D printing process for concentrations of 0.1% w w^{-1} and 1.0% w w^{-1}, while for the sample with 5.0% w w^{-1} of copper clusters a decrease in double bonds conversion can be noticed. These results are in good agreement with the conversion trends obtained for UV-cured coatings [38] and the photorheology data here reported. Despite the lower values, it should be noted that the higher conversions in literature were obtained for longer irradiations and in nitrogen atmosphere, while 3D printing involves very short irradiation times and may suffer of oxygen inhibition, especially in external surfaces. Nevertheless, the measured values are compatible with an efficient 3D printing process and the obtained samples have a very low amount of uncured monomers, as demonstrated by gel content measurements (Table 1).

The thermal properties of the 3D printed materials were also investigated by DSC and TGA tests. Those demonstrated that the introduction of the clusters induces an increase of the glass transition temperature (T_g), probably related to increased hindering of chains movements by the clusters and slight reduction of thermal stability. As reported in Table 1 the T_g raises nearly 10 °C by just adding 0.1% w w^{-1} of 2. This means that the introduction of copper iodide clusters affects the stiffness of the polymeric network (Fig. S8). TGA analyses demonstrated that copper clusters do not affect the thermal stability of the final 3DP devices (Fig. S9).

The photoluminescence of the 3DP polymeric matrix containing 1.0% w w^{-1} of 2 were evaluated. As expected, the material exhibits a large Stokes shift (Fig. 4a) and a thermochromic luminescence, characterized by two temperature-dependent emissions (Fig. 4b) typical of [Cu$_4$I$_4$L$_4$] copper iodide clusters [38,39]. Under UV excitation (330 nm) at room temperature, the printed composite displays a single bright yellow luminescence. This low-energy band (LE) is attributed to a ''cluster-centered'' triplet excited state (3CC) and is independent of the nature of the ligand. Lowering the temperature to 77 K, a structured deep-blue emission appears at higher energy (high-energy band, HE), alongside the LE band. The HE band is assigned to an iodide-to-phosphine ligand charge-transfer transition (XLCT) [51]. The yellow emission is completely recovered when the sample is warmed up, indicating a perfectly reversible thermochromism. Varying the temperature, the emission curves evidence an isosbestic point at 520 nm, indicating a thermal equilibrium between the LE and HE excited states. This implies a very high coupling of the two emission states leading to a perfectly controlled thermochromic luminescence, in a large temperature range.

The quantum yields (QY) were calculated on polymeric films containing 5.0% w w^{-1}, 1.0% w w^{-1} and 0.1% w w^{-1} of copper complex. The measured QY (excitation wavelength 330 nm) of the luminescent material decreases from 60% to 30–10%, decreasing the concentration of the embedded emitter. The values obtained for the 5.0% w w^{-1} polymeric films correspond with the ones reported in literature for the crystalline solid states [39,44,52]. On the other hand, the lower values measured decreasing the emitter amount could be addressed to the concurrent absorption of the polymeric matrix at the exciting wavelength, as demonstrated in Fig. 3c (gray line) and in Fig. S6.
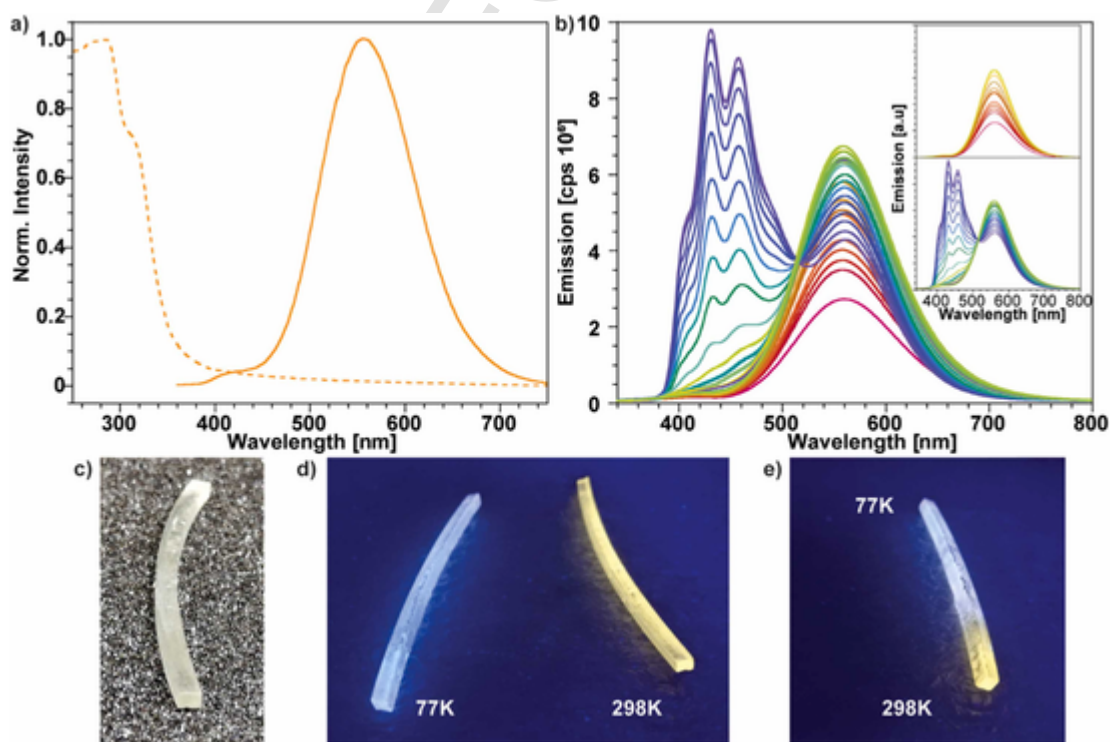
Table 1

Double bond conversions of 3DP films are reported before and after the post curing process in UV oven for 5 s each side. T_g and thermal degradation properties of the final post cured BEDA (blank) and polymers containing different concentrations of 2 (T_5 correspond to the temperatures at which the samples lose 5.0% w w^{-1} of weight) are described.

Compound 2 content [%]	-C=C- Conversion post cured film[a] [%]	Insoluble fraction [%]	T_g [°C]	T_5 [°C]
Blank	80	99	35.4	313
0.1	79	99	48.4	274
1.0	78	99	43.5	288
5.0	70	95	47.1	247

Fig. 4. a) Absorption (dashed) and emission (solid) spectra of 3DP film containing 1.0% w w^{-1} of 2. b) Temperature-dependent luminescence spectra of 2 (λ_{ex} = 330 nm, temperature from room temperature to 77 K). The two insets reported the separated first (top) and second (bottom) emission wavelengths. 3DP polymeric waveguide under ambient light (c), under UV (365 nm) light at different temperatures (77 K and 298 K) and partially immersed in liquid nitrogen (e).

The lifetime of the HE and LE excited states have been also evaluated by time-correlated single photon counting. The measured lifetimes for the two emissions are $\tau LE(RT/77~K) = 9~\mu s$, $\tau^1 HE(77~K) = 0.6~ms$, $\tau^2 HE(77~K) = 3.3~ms$, in accordance with the phosphorescent nature of the two triplet excited states. The results obtained on the 3DP polymeric matrix confirm those previously reported for the fluorophore 2 incorporated in acrylic materials [38]. This is a clear indication that the integrity of the embedded clusters is preserved during the whole DLP process.

Temperature-dependent emission was also clearly detectable as demonstrated below. The 3DP component (Fig. 4c) containing 1.0% w w^{-1} of 2 was irradiated and completely (Fig. 4d) or partially (Fig. 4e) immersed in liquid nitrogen. It is possible to observe with naked eyes the difference in the emission, which suggests also a possible exploitation of this 3DP structures as optical sensor for cryogenic temperatures.

Then, to evaluate the resolution of the final devices, more complex shapes were 3DP using the same optimized parameter, demonstrating the possibility to print very complex structures (Fig. 5a) that keep the peculiar photoluminescent properties of the cluster (Fig. 5b). The light diffuser structure was also investigated by 3D scanner, to evaluate the CAD fidelity. In Fig. 5c a comparison between the CAD virtual project (Fig. S10) and the 3D image of the real 3DP device is depicted, showing the great resolution and fidelity to the project with a displacement at about ± 0.050 mm in the green zones and ± 0.100 mm in the yellow and light blue one. The most evident defects are in the bottom part that represents the first layers built during the printing process (Fig. S11). Those layers are over exposed to ensure the adhesion of the growing object to the printing platform, inducing polymerization even outside the irradiated areas, leading to loss of precision. Regarding the inner parts, those are blind points for the 3D scanner, so that volume cannot be considered meaningful for fidelity evaluation. The displacement data are reported on the top part of Fig. 5c.

We demonstrated the versatility and the good quality and fidelity with the 3D model of the 3DP devices containing copper clusters, fabricating a complex-shaped object: under UV irradiation this device is able to diffuse yellow visible light and it can be used as a downshifter of UV

LEDs, able to change at the same time its photoluminescent properties according to the temperature.

3DP PWGs with different lengths containing 1.0% w w^{-1} of 2 were fabricated to evaluate the conversion of UV irradiation given by a 365 nm LED into visible light and the guiding efficiency through the polymeric matrix. The lengths used were 2, 3 and 5 cm, which is the maximum that can be carried out due to the configuration of the 3D printer used.

Two different configurations, called direct and side pumping, were investigated changing the position of the UV source to evaluate the guiding properties. Sketch representations of these experimental setups are reported in Fig. S12. The measurement conditions of each sample, the voltage used and the relative incident power density are reported in Table S1.

The emitting properties were also studied to evaluate the effective absorption of the UV LED irradiation by the copper cluster, the guiding through the polymeric matrix and the emission of visible irradiation at the end of the PWG for both configurations. The spectra obtained with direct and side pumping configuration are depicted in Fig. 6a-b while the emission of UV LED centered at 365 nm is reported in Fig. S13. The ratio between LED and visible peaks areas are depicted in inset of Fig. 6a in which a reduction of LED intensity and the relative increase of the visible irradiation is clearly visible. In fact, for the direct pumping configuration, the LED peak decreases with the length of the PWG due to the progressive absorption of the irradiation by the copper clusters and, in consequence, the visible irradiation intensity increases. Vice versa, for side pumping geometry the LED irradiation is not visible since the shorter length. Nevertheless, the direct pumping as well as the presence of the LED emission, present a reduction of the visible irradiation according to the increase of the PWG length, while the side pumping shows a reduced lateral dispersion of the irradiation (the blank emission spectra of 3DP PWG for both configurations are depicted in Fig. S14 are the experimental conditions are described in Table S2).

Moreover, an evaluation of the effect of temperature using the direct configuration setup is also reported in Fig. 7, using a Peltier cell to cool the PWG from 40 °C to almost 13 °C (the experimental setup is reported in Fig. S15 and the experimental conditions are reported in Table S3).
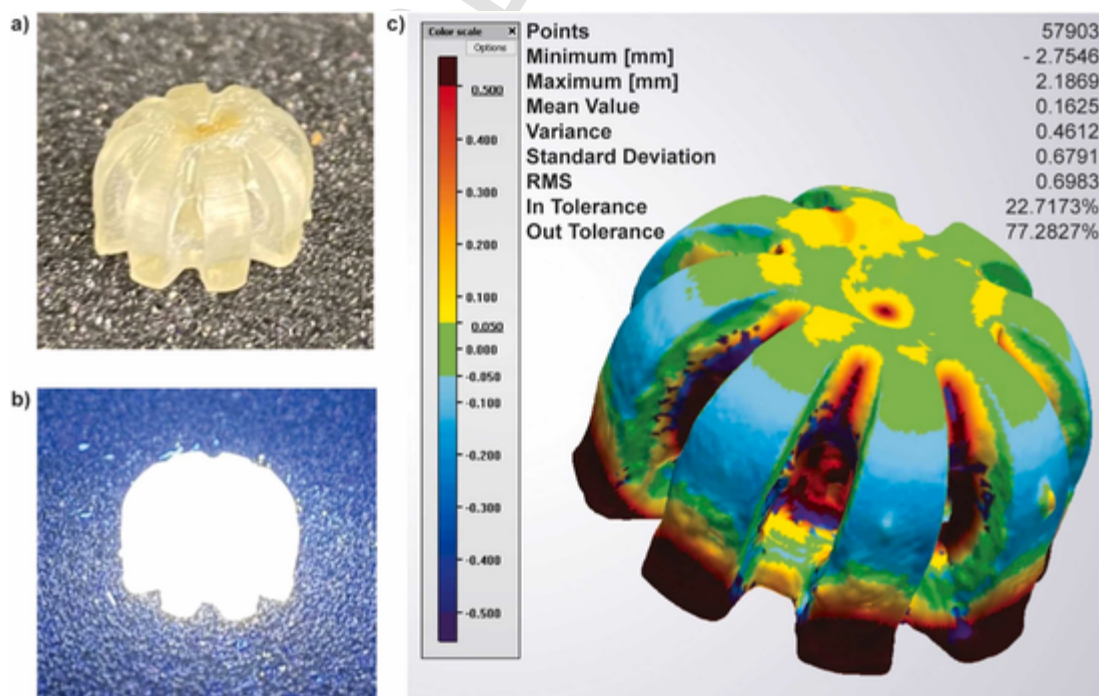

Points	57903
Minimum [mm]	- 2.7546
Maximum [mm]	2.1869
Mean Value	0.1625
Variance	0.4612
Standard Deviation	0.6791
RMS	0.6983
In Tolerance	22.7173%
Out Tolerance	77.2827%

Fig. 5. 3DP device with 1.0% w w^{-1} of 2 (a) under ambient and (b) 365 nm UV light. c) The 3D image obtained with 3D scanner with the evaluation of the displacement between the CAD project and the real device.
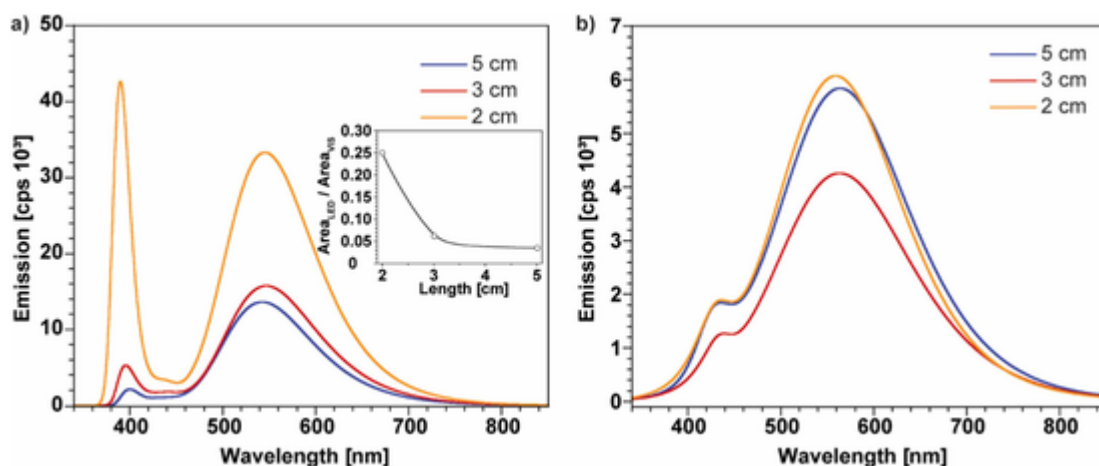
Fig. 6. Emission spectra of (a) direct and (b) side pumping configurations of PWGs with different lengths. In the inset of (a) the ratios between the LED and visible emission areas are reported showing a clear disappearance of the LED's contribution and an increase of visible one.
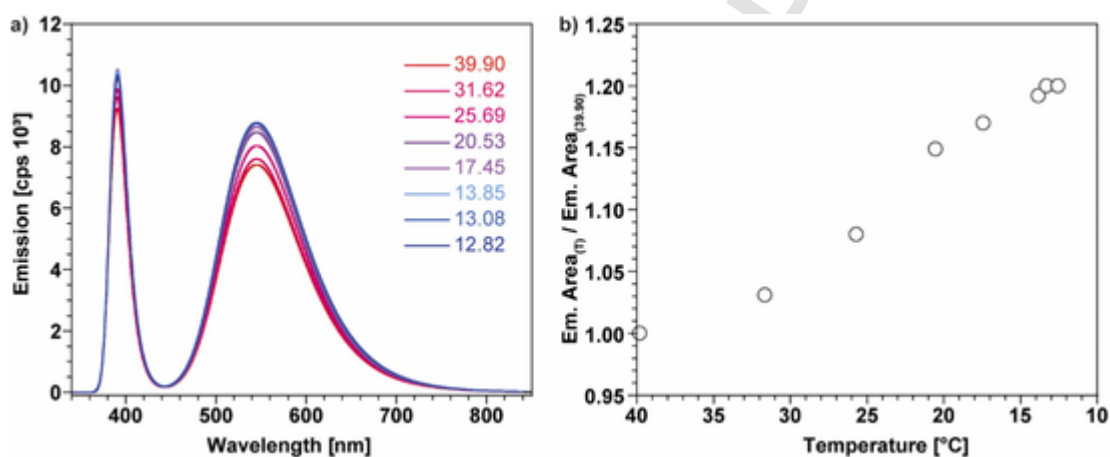

Fig. 7. a) Emission spectra at different temperatures for 2 cm length PWG. b) The normalized emission areas at each temperature over the 39.90 ˚C area to demonstrate a reduction in the emitting properties of the PWGs under increasing of temperature.

In the graph the correlation between the area of each peak and the temperature is reported, showing an increase of the emission, as expected when the temperature decreases, even remaining in the almost common everyday temperature range.

From the previously reported graphs, the guiding of the irradiation is demonstrated, giving promising initial results that can path the way to improvements and other investigations in this field.

4. Conclusion

In this study, the application of copper-based clusters in 3D printable formulations to produce 3D printable photoluminescent devices is reported. The use of this compounds is of particular interest since it allows to avoid the use of more-known rare earth or transition metals complexes, which show synthetic issues, toxicity and higher costs than copper clusters. The embedding of such cluster in 3D printable polymers was demonstrated to be effective, producing materials that show both the emitting properties of the dye and the transparency of the polymeric matrix. Furthermore, thanks to the positive effect of the dye, high resolutions and complex shapes can be achieved in DLP 3D printer, obtaining devices that can be suitable as UV downshifter and as light diffusor. The efficiency of light guiding both for direct and side pumping UV irradiation is investigated, demonstrating initial promising results toward the use of these compounds in PWGs applications: optimal lengths of the device and improvements in the polymeric matrices are needed to achieve more optical transparency and higher guiding effi-

ciency. Temperature-dependency of the emitting properties can lead toward applications even at very low temperature with a change in the emitting wavelengths.

CRediT authorship contribution statement

Matteo Gastaldi: Investigation, Writing – original draft. **Ignazio Roppolo:** Writing – review & editing, Writing – original draft, Supervision, Methodology, Investigation, Conceptualization. **Annalisa Chiappone:** Writing – review & editing, Formal analysis, Data curation. **Claudio Garino:** Writing – review & editing, Investigation, Data curation. **Andrea Fin:** Formal analysis, Writing – review & editing. **Matteo Manachino:** Writing – review & editing, Investigation. **Paolo Sirianni:** Data curation, Investigation, Writing – review & editing. **Guido Viscardi:** Writing – review & editing, Funding acquisition. **Luciano Scaltrito:** Funding acquisition, Methodology, Writing – review & editing. **Marco Zanetti:** Writing – review & editing, Resources. **Silvia Bordiga:** Funding acquisition, Writing – review & editing. **Claudia Barolo:** Writing – review & editing, Supervision, Funding acquisition.

Declaration of Competing Interest

The authors declare the following financial interests/personal relationships which may be considered as potential competing interests:Claudia Barolo reports financial support was provided by Piedmont Region.

Appendix A. Supporting information

Supplementary data associated with this article can be found in the online version at doi:10.1016/j.addma.2021.102504.

References

[1] C.J. Yoo, J.Y. Park, J.-L. Lee, Polymeric nano-pyramids structure for enhancing light extraction in GaN-based LEDs, ECS J. Solid State Sci. Technol. 7 (2018) R190–R193, https://doi.org/10.1149/2.0341811jss.

[2] S. Nocentini, D. Martella, C. Parmeggiani, D.S. Wiersma, 3D printed photoresponsive materials for photonics, Adv. Opt. Mater. 7 (2019) 1900156, https://doi.org/10.1002/adom.201900156.

[3] H. Xia, J. Cheng, L. Zhu, K. Xie, Q. Zhang, D. Zhang, G. Zou, One-dimensional programmable polymeric microfiber waveguide with optically reconfigurable photonic functions, ACS Appl. Mater. Interfaces 11 (2019) 15969–15976, https://doi.org/10.1021/acsami.8b22140.

[4] C.-L. Sun, Z. Gao, K.-X. Teng, L.-Y. Niu, Y.-Z. Chen, Y.S. Zhao, Q.-Z. Yang, Supramolecular polymer-based fluorescent microfibers for switchable optical waveguides, ACS Appl. Mater. Interfaces 10 (2018) 26526–26532, https://doi.org/10.1021/acsami.8b08490.

[5] H. Ma, A.K.-Y. Jen, L.R. Dalton, Polymer-based optical waveguides: materials, processing, and devices, Adv. Mater. 14 (2002) 1339–1365, https://doi.org/10.1002/1521-4095(20021002)14:19<1339::AID-ADMA1339>3.0.CO;2-O.

[6] J.W. Choi, Y.M. Ha, S.H. Lee, K.H. Choi, Design of microstereolithography system based on dynamic image projection for fabrication of three-dimensional microstructures, J. Mech. Sci. Technol. 20 (2006) 2094–2104, https://doi.org/10.1007/BF02916326.

[7] J. Feng, Q. Jiang, P. Rogin, P.W. de Oliveira, A. del Campo, Printed soft optical waveguides of PLA copolymers for guiding light into tissue, ACS Appl. Mater. Interfaces 12 (2020) 20287–20294, https://doi.org/10.1021/acsami.0c03903.

[8] J. Guo, C. Yang, Q. Dai, L. Kong, Soft and stretchable polymeric optical waveguide-based sensors for wearable and biomedical applications, Sens. (Basel). 19 (2019) 3771, https://doi.org/10.3390/s19173771.

[9] J. Alamán, M. López-Valdeolivas, R. Alicante, C. Sánchez-Somolinos, Optical Planar Waveguide Sensor with Integrated Digitally-Printed Light Coupling-in and Readout Elements, Sensors 19 (2019), https://doi.org/10.3390/s19132856.

[10] K. Jakubowski, W. Kerkemeyer, E. Perret, M. Heuberger, R. Hufenus, Liquid-core polymer optical fibers for luminescent waveguide applications, Mater. Des. 196 (2020) 109131, https://doi.org/10.1016/j.matdes.2020.109131.

[11] D. Niu, L. Wang, Q. Xu, M. Jiang, X. Wang, X. Sun, F. Wang, D. Zhang, Ultra-sensitive polymeric waveguide temperature sensor based on asymmetric Mach–Zehnder interferometer, Appl. Opt. 58 (2019) 1276–1280, https://doi.org/10.1364/AO.58.001276.

[12] S.-H. Oh, K.-D. Ahn, H.-Y. Choi, Fabrication of fluorescent oxygen gas-sensor probe module based on asymmetric 1 × 2 optical waveguides using UV imprint lithography, Opt. Eng. 58 (2019) 1, https://doi.org/10.1117/1.OE.58.9.097104.

[13] T.Y. Hin, C. Liu, P.P. Conway, A Review on 3D Integrated Approaches in Multimode Optical Polymeric Waveguide Fabrication, in 2007 Proceedings 57th Electronic Components and Technology Conference, 2007: pp. 1737–1741. https://doi.org/10.1109/ECTC.2007.374030.

[14] V. Fasano, M. Moffa, A. Camposeo, L. Persano, D. Pisignano, Controlled atmosphere electrospinning of organic nanofibers with improved light emission and waveguiding properties, Macromolecules 48 (2015) 7803–7809, https://doi.org/10.1021/acs.macromol.5b01377.

[15] H. Xia, T. Chen, C. Hu, K. Xie, Recent advances of the polymer micro/nanofiber fluorescence waveguide, Polymers 10 (2018) 1086, https://doi.org/10.3390/polym10101086.

[16] C.A. Briehn, M.-S. Schiedel, E.M. Bonsen, W. Schuhmann, P. Bäuerle, Single-compound libraries of organic materials: from the combinatorial synthesis of conjugated oligomers to structure–property relationships, Angew. Chem. Int. Ed. 40 (2001) 4680–4683, https://doi.org/10.1002/1521-3773(20011217)40:24<4680::AID-ANIE4680>3.0.CO;2-X.

[17] C. Gu, N. Huang, Y. Chen, L. Qin, H. Xu, S. Zhang, F. Li, Y. Ma, D. Jiang, π-conjugated microporous polymer films: designed synthesis, conducting properties, and photoenergy conversions, Angew. Chem. Int. Ed. 54 (2015) 13594–13598, https://doi.org/10.1002/anie.201506570.

[18] A. Garreau, J.-L. Duvail, Recent advances in optically active polymer-based nanowires and nanotubes, Adv. Opt. Mater. 2 (2014) 1122–1140, https://doi.org/10.1002/adom.201400232.

[19] S. Hayashi, Elastic organic crystals of π-conjugated molecules: anisotropic densely packed supramolecular 3D polymers exhibit mechanical flexibility and shape tunability, Polym. J. 51 (2019) 813–823, https://doi.org/10.1038/s41428-019-0201-8.

[20] F. Wang, Y. Chong, F. Wang, C. He, Photopolymer resins for luminescent three-dimensional printing, J. Appl. Polym. Sci. 134 (2017) 44988, https://doi.org/10.1002/app.44988.

[21] M. Nadgorny, A. Ameli, Functional polymers and nanocomposites for 3d printing of smart structures and devices, ACS Appl. Mater. Interfaces 10 (2018) 17489–17507, https://doi.org/10.1021/acsami.8b01786.

[22] J.A. Lewis, Direct ink writing of 3D functional materials, Adv. Funct. Mater. 16 (2006) 2193–2204, https://doi.org/10.1002/adfm.200600434.

[23] M. Gastaldi, F. Cardano, M. Zanetti, G. Viscardi, C. Barolo, S. Bordiga, S. Magdassi, A. Fin, I. Roppolo, Functional dyes in polymeric 3D printing: applications and perspectives, ACS Mater. Lett. (2020) 1–17, https://doi.org/10.1021/acsmaterialslett.0c00455.

[24] R. Stach, J. Haas, E. Tütüncü, S. Daboss, C. Kranz, B. Mizaikoff, polyHWG: 3D printed substrate-integrated hollow waveguides for mid-infrared gas sensing, ACS Sens 2 (2017) 1700–1705, https://doi.org/10.1021/acssensors.7b00649.

[25] S. Khan, N. Vahabisani, M. Daneshmand, A fully 3-d printed waveguide and its application as microfluidically controlled waveguide switch, IEEE Trans. Compon. Packag. Manuf. Technol. 7 (2017) 70–80, https://doi.org/10.1109/TCPMT.2016.2631545.

[26] F. Zhao, D. Cambié, J. Janse, E.W. Wieland, K.P.L. Kuijpers, V. Hessel, M.G. Debije, T. Noël, Scale-up of a luminescent solar concentrator-based photomicroreactor via numbering-up, ACS Sustain. Chem. Eng. 6 (2018) 422–429, https://doi.org/10.1021/acssuschemeng.7b02687.

[27] Q. Mu, C.K. Dunn, L. Wang, M.L. Dunn, H.J. Qi, T. Wang, Thermal cure effects on electromechanical properties of conductive wires by direct ink write for 4D printing and soft machines, Smart Mater. Struct. 26 (2017) 045008, https://doi.org/10.1088/1361-665X/aa5cca.

[28] N. Huby, J. Bigeon, Q. Lagneaux, M. Amela-Cortes, A. Garreau, Y. Molard, J. Fade, A. Desert, E. Faulques, B. Bêche, J.-L. Duvail, S. Cordier, Facile design of red-emitting waveguides using hybrid nanocomposites made of inorganic clusters dispersed in SU8 photoresist host, Opt. Mater. 52 (2016) 196–202, https://doi.org/10.1016/j.optmat.2015.12.034.

[29] Y. Xia, B. Xue, M. Qin, Y. Cao, Y. Li, W. Wang, Printable fluorescent hydrogels based on self-assembling peptides, Sci. Rep. 7 (2017) 1–10, https://doi.org/10.1038/s41598-017-10162-y.

[30] Y. Ren, J. Feng, Skin-inspired multifunctional luminescent hydrogel containing layered rare-earth hydroxide with 3D printability for human motion sensing, ACS Appl. Mater. Interfaces 12 (2020) 6797–6805, https://doi.org/10.1021/acsami.9b17371.

[31] S. Moynihan, R. Van Deun, K. Binnemans, G. Redmond, Optical properties of planar polymer waveguides doped with organo-lanthanide complexes, Opt. Mater. 29 (2007) 1821–1830, https://doi.org/10.1016/j.optmat.2006.10.005.

[32] Z. Li, P. Liu, X. Ji, J. Gong, Y. Hu, W. Wu, X. Wang, H.-Q. Peng, R.T.K. Kwok, J.W.Y. Lam, J. Lu, B.Z. Tang, Bioinspired simultaneous changes in fluorescence color, brightness, and shape of hydrogels enabled by aIEgens, Adv. Mater. 32 (2020) 1906493, https://doi.org/10.1002/adma.201906493.

[33] D. Ahn, L.M. Stevens, K. Zhou, Z.A. Page, Rapid high-resolution visible light 3D printing, ACS Cent. Sci. 6 (2020) 1555–1563, https://doi.org/10.1021/acscentsci.0c00929.

[34] F. Frascella, G. González, P. Bosch, A. Angelini, A. Chiappone, M. Sangermano, C.F. Pirri, I. Roppolo, Three-dimensional printed photoluminescent polymeric waveguides, ACS Appl. Mater. Interfaces 10 (2018) 39319–39326, https://doi.org/10.1021/acsami.8b16036.

[35] I. Roppolo, A. Chiappone, A. Angelini, S. Stassi, F. Frascella, C.F. Pirri, C. Ricciardi, E. Descrovi, 3D printable light-responsive polymers, Mater. Horiz. 4 (2017) 396–401, https://doi.org/10.1039/C7MH00072C.

[36] M. Gillono, I. Roppolo, F. Frascella, L. Scaltrito, C.F. Pirri, A. Chiappone, CO₂ permeability control in 3D printed light responsive structures, Appl. Mater. Today 18 (2020) 100470, https://doi.org/10.1016/j.apmt.2019.100470.

[37] H. Xie, K.-K. Yang, Y.-Z. Wang, Photo-cross-linking of anthracene as a versatile strategy to design shape memory polymers, Mater. Today Proc. 16 (2019) 1524–1530, https://doi.org/10.1016/j.matpr.2019.05.335.

[38] I. Roppolo, E. Celasco, A. Fargues, A. Garcia, A. Revaux, G. Dantelle, F. Maroun, T. Gacoin, J.-P. Boilot, M. Sangermano, S. Perruchas, Luminescence thermochromism of acrylic materials incorporating copper iodide clusters, J. Mater. Chem. 21 (2011) 19106–19113, https://doi.org/10.1039/C1JM13600C.

[39] S. Perruchas, X.F. Le Goff, S. Maron, I. Maurin, F. Guillen, A. Garcia, T. Gacoin, J.-P. Boilot, Mechanochromic and thermochromic luminescence of a copper iodide cluster, J. Am. Chem. Soc. 132 (2010) 10967–10969, https://doi.org/10.1021/ja103431d.

[40] B. Li, H.-T. Fan, S.-Q. Zang, H.-Y. Li, L.-Y. Wang, Metal-containing crystalline luminescent thermochromic materials, Coord. Chem. Rev. 377 (2018) 307–329, https://doi.org/10.1016/j.ccr.2018.09.004.

[41] B. Xin, J. Sang, Y. Gao, G. Li, Z. Shi, S. Feng, A pillared-layered copper(I) halide-based metal–organic framework exhibiting dual emission, and piezochromic and thermochromic properties with a large temperature-dependent emission red-shift, RSC Adv. 8 (2018) 1973–1978, https://doi.org/10.1039/C7RA11950J.

[42] E. Cariati, E. Lucenti, C. Botta, U. Giovanella, D. Marinotto, S. Righetto, Cu(I) hybrid inorganic–organic materials with intriguing stimuli responsive and optoelectronic properties, Coord. Chem. Rev. 306 (2016) 566–614, https://doi.org/10.1016/j.ccr.2015.03.004.

[43] B. Huitorel, H. El Moll, R. Utrera-Melero, M. Cordier, A. Fargues, A. Garcia, F. Massuyeau, C. Martineau-Corcos, F. Fayon, A. Rakhmatullin, S. Kahlal, J.-Y. Saillard, T. Gacoin, S. Perruchas, Evaluation of ligands effect on the photophysical properties of copper iodide clusters, Inorg. Chem. 57 (2018) 4328–4339, https://doi.org/10.1021/acs.inorgchem.7b03160.

[44] C. Tard, S. Perruchas, S. Maron, X.F. Le Goff, F. Guillen, A. Garcia, J. Vigneron, A.

Etcheberry, T. Gacoin, J.-P. Boilot, Thermochromicluminescence of Sol–gel films based on copper iodide clusters, Chem. Mater. 20 (2008) 7010–7016, https://doi.org/10.1021/cm801780g.

[45] Q. Benito, I. Maurin, T. Cheisson, G. Nocton, A. Fargues, A. Garcia, C. Martineau, T. Gacoin, J.-P. Boilot, S. Perruchas, Mechanochromic luminescence of copper iodide clusters, Chem. A Eur. J. 21 (2015) 5892–5897, https://doi.org/10.1002/chem.201500251.

[46] A.V. Shamsieva, I.E. Kolesnikov, I.D. Strelnik, T.P. Gerasimova, A.A. Kalinichev, S.A. Katsyuba, E.I. Musina, E. Lähderanta, A.A. Karasik, O.G. Sinyashin, Fresh look on the nature of dual-band emission of octahedral copper-iodide clusters—promising ratiometric luminescent thermometers, J. Phys. Chem. C 123 (2019) 25863–25870, https://doi.org/10.1021/acs.jpcc.9b07603.

[47] B. Huitorel, H. El Moll, M. Cordier, A. Fargues, A. Garcia, F. Massuyeau, C. Martineau-Corcos, T. Gacoin, S. Perruchas, Luminescence mechanochromism induced by cluster isomerization, Inorg. Chem. 56 (2017) 12379–12388, https://doi.org/10.1021/acs.inorgchem.7b01870.

[48] Q.-W. Guan, D. Zhang, Z.-Z. Xue, X.-Y. Wan, Z.-N. Gao, X.-F. Zhao, C.-P. Wan, J. Pan, G.-M. Wang, Structural characterization, photoluminescence and sensing properties of two copper(I)-iodide compounds, Inorg. Chem. Commun. 95 (2018) 144–148, https://doi.org/10.1016/j.inoche.2018.07.022.

[49] S. Perruchas, C. Tard, X.F. Le Goff, A. Fargues, A. Garcia, S. Kahlal, J.-Y. Saillard, T. Gacoin, J.-P. Boilot, Thermochromic Luminescence of Copper Iodide Clusters: The Case of Phosphine Ligands, Inorg. Chem. 50 (2011) 10682–10692, https://doi.org/10.1021/ic201128a.

[50] B. Huitorel, R. Utrera-Melero, F. Massuyeau, J.-Y. Mevelec, B. Baptiste, A. Polian, T. Gacoin, C. Martineau-Corcos, S. Perruchas, Luminescence mechanochromism of copper iodide clusters: a rational investigation, Dalton Trans. 48 (2019) 7899–7909, https://doi.org/10.1039/C9DT01161G.

[51] F. De Angelis, S. Fantacci, A. Sgamellotti, E. Cariati, R. Ugo, P.C. Ford, Electronic transitions involved in the absorption spectrum and dual luminescence of tetranuclear cubane [Cu4I4(pyridine)4] cluster: a density functional theory/time-dependent density functional theory investigation, Inorg. Chem. 45 (2006) 10576–10584, https://doi.org/10.1021/ic061147f.

[52] S. Perruchas, C. Tard, X.F. Le Goff, A. Fargues, A. Garcia, S. Kahlal, J.-Y. Saillard, T. Gacoin, J.-P. Boilot, Thermochromic luminescence of copper iodide clusters: the case of phosphine ligands, Inorg. Chem. 50 (2011) 10682–10692, https://doi.org/10.1021/ic201128a.